

## Fluctuations and Phase Separation in a Quasi-One-Dimensional System

Enrico Doná, Thomas Loerting, Simon Penner, Mariana Minca, Alexander Menzel, and Erminald Bertel  
*Institute of Physical Chemistry, University of Innsbruck, Innrain 52a, A-6020 Innsbruck, Austria*

Johannes Schoiswohl, Steven Berkebile, and Falko P. Netzer  
*Institute of Experimental Physics, University of Graz, Universitätsplatz 5, A-8010 Graz, Austria*

Rinaldo Zucca and Josef Redinger  
*Center for Computational Materials Science, Vienna University of Technology, Getreidemarkt 9/134, A-1060 Vienna, Austria*  
(Received 22 December 2006; published 1 May 2007)

Phase transitions in a quasi-one-dimensional surface system on a metal substrate are investigated as a function of temperature. Upon *cooling* the system shows a loss of long-range order, fluctuations, and a transition into an inhomogeneous ground state due to competition of local adsorbate-adsorbate interactions with an incommensurate charge density wave. This agrees with a general phase diagram for correlated systems and high-temperature superconductors. The model surface system allows direct imaging of the fluctuations and the glassy inhomogeneous ground state by scanning tunneling microscopy.

DOI: [10.1103/PhysRevLett.98.186101](https://doi.org/10.1103/PhysRevLett.98.186101)

PACS numbers: 68.35.Rh, 68.37.Ef, 68.43.Bc

Correlated systems exhibit a rich phase diagram with competing order parameters [1] and electronically driven phase transitions. Changes in doping, pressure, or chemical composition can give rise to quantum phase transitions (QPTs) [2] at  $T = 0$  K. Experimental examination of the competing phases has to cope with intense fluctuations at  $T > 0$  and a tendency to phase separation [3,4]. The interest in QPTs is partly driven by the high-temperature superconductors (HTSCs), where magnetic order and charge order compete with superconductivity. This competition results in the loss of long-range order and a phase separation [5] into conducting, hole-rich stripes embedded in an antiferromagnetic, Mott-insulating background [6–8]. Fluctuations, commonly occurring around the critical temperature of one of the order parameters [9,10], are believed to be also at the origin of the pseudogap phase in the HTSCs. In this work we present a surface system, i.e.,  $c(2 \times 2)$ -Br/Pt(110), which exhibits several characteristics of correlated systems. In particular, we find a competition of different order parameters at low temperature and strong fluctuations. Lowering the temperature yields a transition from a long-range ordered phase into a strongly fluctuating and finally into an inhomogeneous state. As the system is accessible by surface sensitive methods and, in particular, by direct imaging in scanning tunneling microscopy (STM), an unprecedented insight is provided into how an inhomogeneous, striped phase evolves out of a well-ordered phase as the temperature is reduced.

Our model system is the  $c(2 \times 2)$ -Br/Pt(110) surface [11,12] [see Fig. 1(a) and 1(b); other surface structures mentioned below are also defined in Fig. 1(b)]. This long-range ordered room-temperature phase is obtained at a coverage  $\Theta_{\text{Br}} = 0.5$  monolayers [ML; 1 ML corresponds to the density of surface atoms on a  $(1 \times 1)$ -Pt(110) surface]. The preparation has been described previously [13].

A small increase in coverage was found to result in fluctuations and an apparent  $(3 \times 1)$  phase, which we attributed to the formation of a charge density wave (CDW) with threefold periodicity [14]. Exploration of the phase diagram as a function of temperature is nontrivial, because close to critical temperatures the system is expected to exhibit rapid fluctuations not observable in the time-averaged STM contrast. However, from low-energy electron diffraction (LEED) spot profiles the  $T$  dependence of the long-range order parameter, the intensity of fluctuations and their correlation length can be extracted. The analysis is based on the customary decomposition of the structure factor near a critical temperature into three components [15,16]:

$$S(q, T) = I_0(T) * \delta(q - q_0) + \chi_0(T) / [1 + \xi^2(T) * (q - q_0)^2] + \text{background}.$$

$I_0$  is the intensity of the Bragg peak scaling with the square of the order parameter,  $q$  refers to a momentum-space vector,  $q_0$  is the center of the LEED spot,  $\chi_0$  is the generalized susceptibility, and  $\xi$  is the correlation length. In practice, the first component is broadened into a Gaussian due to finite terrace width and instrumental resolution. The height of the Gaussian yields the  $T$  dependence of the long-range order parameter after correction for the Debye-Waller factor. The second part is a Lorentzian function characterizing fluctuations in the system. As the interactions along and perpendicular to the close-packed rows are vastly different [12], a separate analysis for both directions was carried out. To test the reliability and reproducibility of the experimental decomposition we analyzed two different sets of measurements. One was recorded using a normal LEED system equipped with a high-sensitivity CCD camera. Beam currents were below 1 nA

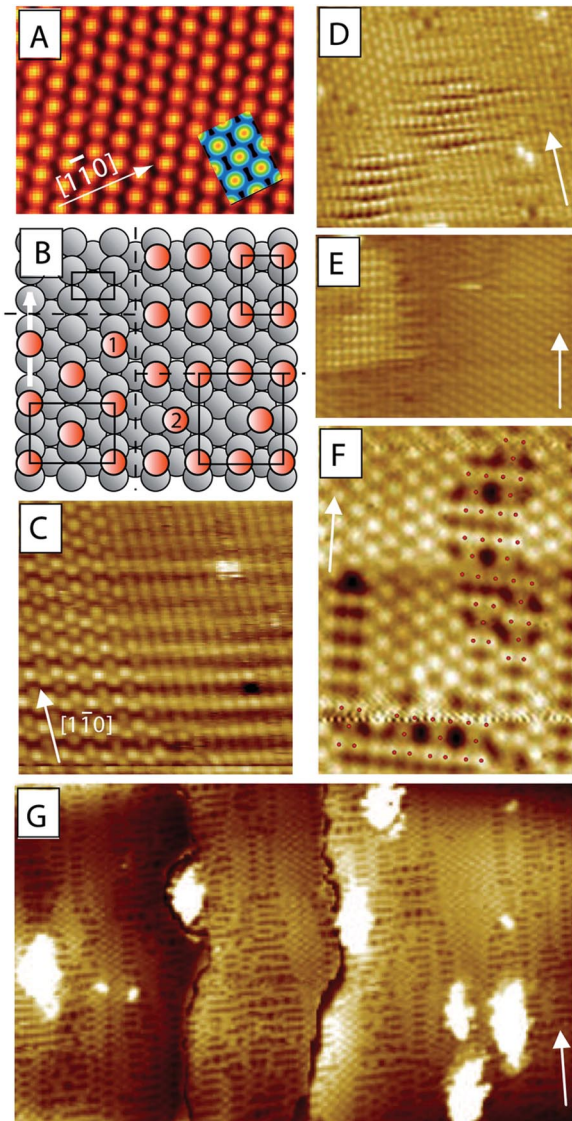


FIG. 1 (color). (a) STM image of the  $c(2 \times 2)$ -Br/Pt(110) surface ( $T = 300$  K,  $55 \times 41 \text{ \AA}^2$ ,  $0.63$  V,  $1.13$  nA). White arrows mark the direction of the close-packed Pt rows. The inset shows a simulated STM image based on DFT calculations and displaying contours of constant charge density. (b) Ball model of the Pt(110) surface (gray balls) with the  $(1 \times 1)$  unit cell (upper left), as well as Br (orange balls)  $c(2 \times 2)$  (lower left),  $(2 \times 1)$  (upper right), and  $(3 \times 2)$  (lower right) domains. The unit cells are shown as black rectangles, the dashed black lines mark the domain boundaries. Br atom 1 occupies a short-bridge, Br atom 2 a long-bridge site. (c) STM image ( $T = 300$  K,  $75 \times 65 \text{ \AA}^2$ ,  $0.162$  V,  $1.10$  nA) of an area close to a defect (dark spot at lower right of the image). (d) STM image of a  $c(2 \times 2)$  preparation recorded at  $T = 110$  K ( $105 \times 90 \text{ \AA}^2$ ,  $0.92$  V,  $1.96$  nA) showing  $c(2 \times 2)$  and  $(2 \times 1)$  contrast. (e) Different area of the same preparation as shown in (d) ( $T = 110$  K,  $0.84$  V,  $0.12$  nA). (f) STM image of a  $c(2 \times 2)$  preparation recorded at  $T = 50$  K ( $78 \times 59 \text{ \AA}^2$ ), showing in addition  $(3 \times 2)$  structural elements. (g) Large-area STM scan recorded at  $T = 50$  K ( $415 \times 251 \text{ \AA}^2$ ,  $0.51$  V,  $0.33$  nA) showing three terraces separated by monatomic steps.  $c(2 \times 2)$ ,  $(2 \times 1)$  and  $(3 \times 2)$  domains form a striped phase without long-range order.

and the coherence length was 20–25 nm as determined from the spot profiles of the clean Pt(110) surface. The second set was measured with a spot-profile analysis (SPA) LEED featuring a LaB<sub>6</sub> cathode and a coherence length of  $\sim 100$  nm. Both sets yielded qualitatively the same result. The error bars for the Lorentzian and the Gaussian peak height are  $\sim 25\%$  and  $\sim 10\%$ , respectively, apart from temperatures below 200 K and above 450 K, where the total peak intensities were low. The data shown in Fig. 2 refer to the normal LEED system, because in this case the

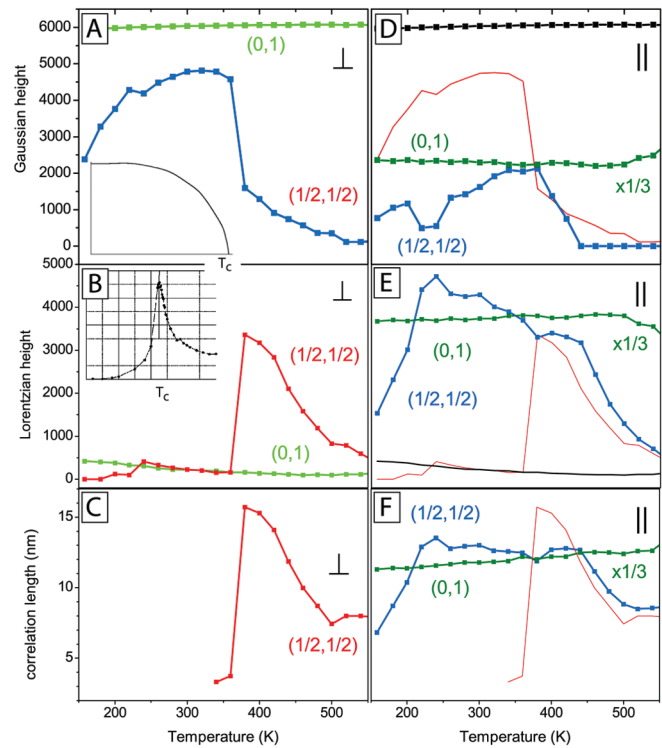


FIG. 2 (color). LEED spot-profile analysis. All peak heights have been corrected by the Debye-Waller factor obtained from the integer-order peak intensity. (a) Height of the Gaussian component in the peak profile measured perpendicular to the close-packed row direction for the  $(1/2, 1/2)$  and the  $(0,1)$  spot. Inset: Theoretical power-law dependence of the order parameter in the Ising model, which is isomorphous to the  $c(2 \times 2)$  structure. (b) Height of the Lorentzian component in the peak profile measured perpendicular to the close-packed row direction for the  $(1/2, 1/2)$  and the  $(0,1)$  spot. Inset: Monte Carlo calculation of critical fluctuations in the Ising model. The divergence at  $T_c$  is rounded off due to the finite size of the grid. (c) Correlation length of the critical fluctuations in the adsorbate system perpendicular to the close-packed row direction. (d) Height of the Gaussian component in the peak profile measured parallel to the close-packed row direction for the  $(1/2, 1/2)$  and the  $(0,1)$  spot. For comparison, the behavior in the orthogonal direction is displayed as the thin red curve. (e) Height of the Lorentzian component in the peak profile measured parallel to the close-packed row direction for the  $(1/2, 1/2)$  and the  $(0,1)$  spot. (f) Correlation length of the critical fluctuations parallel to the close-packed row direction.

measurement was much faster, thus minimizing contamination from the residual gas.

Analysis of Figs. 2(a)–2(c) allows the following conclusions: The fractional-order spot shows critical behavior as  $T$  is raised above 375 K with a precipitous drop of the long-range order and the simultaneous appearance of fluctuations ( $\xi \sim 150$  Å). Residual long-range order at  $T > T_c$  is caused by pinning of the  $c(2 \times 2)$  structure at steps. Towards higher temperatures both the fluctuations and the correlation length drop off. This behavior signals a normal order-disorder transition as illustrated by model calculations shown as inset in Figs. 2(a) and 2(b). The integer-order spot profile perpendicular to the close-packed rows remains unchanged during the order-disorder transition, which indicates that the substrate is not affected. Below 375 K, LEED as well as STM show a long-range ordered  $c(2 \times 2)$  phase, but the spot-profile in  $[1\bar{1}0]$  direction reveals hidden fluctuations: The Lorentzian component in the half-order spot increases as  $T$  is decreased from 375 K and in the integer-order spot it remains larger than the Gaussian contribution throughout the  $T$  range from 375 K down to 250 K. Thus, the substrate surface also fluctuates. The structure, including the substrate surface, is long-range ordered perpendicular, but fluctuates along the close-packed rows with a correlation length of  $\sim 130$  Å [Figs. 2(d)–2(f)]. These fluctuations are not observable by STM on the terraces except around defects, where the threefold periodicity appears [Fig. 1(c)], because the fluctuations are pinned and do not average out. As the STM contrast is due to the adsorbed Br atoms [see Fig. 1(a)], Fig. 1(c) implies that the Br atoms participate in the fluctuations by jumping back and forth between different adsorption sites. According to a structure analysis of the static  $(3 \times 1)$  phase carried out previously [14] the fluctuations in the substrate are associated with a strong substrate buckling.

As the temperature is decreased below 250 K, all LEED spots fade away rather quickly. Hence, analysis of the low- $T$  phase has to rely on STM. Images obtained at 110 K [Figs. 1(d) and 1(e)] show a strongly disturbed  $c(2 \times 2)$  structure and the appearance of  $(2 \times 1)$  domains. The changing and occasionally blurred contrast is typical for STM images of fluctuating phases.

After further cooling to  $\sim 50$  K a coexistence of  $c(2 \times 2)$ ,  $(2 \times 1)$  and a  $(3 \times 2)$  structure is observed in STM. The Br coverage for all these structures is 0.5 ML [Figs. 1(f) and 1(g)]. Apparently the three structures are nearly degenerate at 50 K. This is confirmed by density-functional theory (DFT) [14], which yields only  $\sim 14$  meV/atom difference between  $c(2 \times 2)$ , the  $(2 \times 1)$  and the  $(3 \times 2)$  structure. While one could understand easily that a higher-energy phase is suppressed at low  $T$  and becomes more populated as the temperature is raised, the observation of a disordered glassy phase at low  $T$  and a pure, long-range ordered phase, i.e., the  $c(2 \times 2)$ , at 300 K requires a more sophisticated model.

Improved long-range ordering at higher temperatures can only be explained by temperature dependent interactions. The dominant interaction in the  $c(2 \times 2)$  structure originates from the Br-Br repulsion on nearest-neighbor and next-nearest-neighbor short-bridge sites [for definition of sites see Fig. 1(b)] and yields a quasihexagonal packing of the Br atoms. In addition, however, a Peierls-type  $2k_F$  interaction ( $k_F$  being the Fermi wave vector) favors an incommensurate CDW phase at low  $T$  [14,17]. The incommensurability results in the appearance of both,  $(2 \times 1)$  and  $(3 \times 2)$  domains. The presence of  $(3 \times 2)$  domains at low  $T$  indicates that there long-bridge sites are energetically equivalent to short-bridge sites, while at 300 K they are not. Incommensurate CDWs are predicted not to show a well-defined Peierls transition, but to fluctuate over a wide temperature range and to phase separate into domains with different periodicities [9,10]. The incommensurability is also supported by angle-resolved photoemission experiments, which yield  $1/4G < k_F < 1/3G$  for the relevant surface state ( $G$  being a reciprocal surface lattice vector) [14]. As  $T$  is raised above the Peierls temperature, electrons are increasingly excited across the Peierls gap and the CDW dies out. The less  $T$ -dependent local adsorbate-adsorbate repulsion remains as dominant interaction and stabilizes the global  $c(2 \times 2)$  phase.

In summary, we arrive at the following model: At 50 K, the  $c(2 \times 2)$ , the  $(2 \times 1)$  and the  $(3 \times 2)$  structure are degenerate. The latter two phases are stabilized by the incommensurate Peierls interaction in the Pt top layer. The buckling of this layer, i.e., the frozen Rayleigh phonon, renders the long-bridge site energetically equivalent to the short-bridge sites. Above  $T_{MF}$  (mean-field Peierls temperature) the  $(2 \times 1)$  and the  $(3 \times 2)$  phase are unstable. Fluctuations are thermally excited, but drop off with increasing  $T$  (decreasing Peierls interaction) and an ever better  $c(2 \times 2)$  order develops. Finally, at 375 K the  $c(2 \times 2)$  structure is destroyed as well in a sharp order-disorder transition. This model also refines our previous interpretation of the  $(3 \times 1)$  structure as a CDW [14,17]: The “ $(3 \times 1)$ ” domains observed at  $0.50 < \Theta_{Br} < 0.55$  ML are actually fluctuating  $(3 \times 2)$  CDW domains, whereas the proper  $(3 \times 1)$  structure at  $\Theta_{Br} = 0.67$  ML is according to the DFT calculations higher in energy and, therefore, not a true Peierls phase.

The generic phase diagram of quasi-1D systems shown in Fig. 3 [18] puts the present observations into a wider perspective. The coupling parameter  $t_{\perp}$  (hopping matrix element) establishes phase coherence between the one-dimensional subunits at  $T \ll T_{CH} = t_{\perp}/\pi k_B$  ( $k_B$  being the Boltzmann constant). For  $T > T_{CH}$  (the “coherence temperature”) coherence from row to row is lost. For the  $c(2 \times 2)$  phase  $T_{CH} = 375$  K. Above this temperature long-range order is lost. Below 375 K the  $c(2 \times 2)$  phase prevails, but as  $T$  is lowered towards  $T_{MF}$ , fluctuations intensify. They are coherent from row to row as  $T$  is below

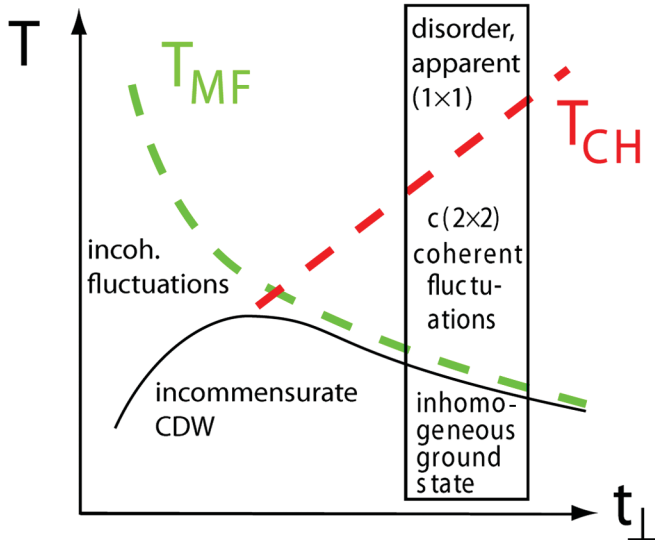


FIG. 3 (color). Generic phase diagram of quasi-one-dimensional systems.  $t_{\perp}$  is the hopping matrix element which couples the 1D subunits.  $T_{MF}$  is the Peierls mean-field temperature which separates the CDW phase ( $T < T_{MF}$ ) from the parent phase ( $T > T_{MF}$ ).  $T_{CH}$  is the coherence temperature above which the coherence between the 1D subunits is lost.

$T_{CH}$ . If  $T$  is reduced further to below  $T_{MF}$ , an inhomogeneous phase develops (in the present case a striped pattern of  $c(2 \times 2)$ ,  $(2 \times 1)$  and  $(3 \times 2)$  structures). Thus, the conceptually simple phase diagram of quasi-1D systems is associated with a rather complex phenomenology in real systems. Intense fluctuations over a large temperature range and eventual phase separation complicate the experimental observation of phase transitions in such systems. The left part of the phase diagram shown in Fig. 3 applies to very weak transverse coupling. Here  $T_{MF}$  is larger than  $T_{CH}$ . Upon cooling below  $T_{MF}$  the Peierls interaction is switched on in individual chains, but with a random phase variation from chain to chain. As long-range order is strongly suppressed in 1D, this phase is characterized by intense fluctuations, which are not correlated from row to row. Only if  $T$  falls below  $T_{CH}$  as well, phase coherence is established and a global CDW phase is formed. Similar considerations apply for 2D systems. In that case,  $t_{\perp}$  refers to the coupling from plane to plane. Fluctuations are less extensive than for quasi-1D systems, but are still important.

In conclusion, the present quasi-1D surface system allows direct imaging of phase transitions typically for correlated systems. The results illustrate how fluctuations dominate the behavior over a wide range of temperatures. Cooling leads to a counterintuitive destruction of a long-range ordered state by phase separation into a glassy ground state. The observations may also be relevant for a better understanding of high-temperature superconductors.

Support by the Austrian Science Funds (FWF) and the nanonetwork WINN is gratefully acknowledged.

- 
- [1] C. Bourbonnais, J. Phys. IV (France) **10**, Pr3-81 (2000).
  - [2] S. Sachdev, Science **288**, 475 (2000).
  - [3] Z. Nussinov, I. Vekhter, and A. Balatsky, cond-mat/0409474.
  - [4] F. Guinea, G. Gómez-Santos, and D.P. Arovas, Phys. Rev. B **62**, 391 (2000).
  - [5] B.P. Stojković, Z. G. Yu, A. L. Chernyshev, A. R. Bishop, A. H. Castro Neto, and N. Grønbech-Jensen, Phys. Rev. B **62**, 4353 (2000).
  - [6] J. Orenstein and A.J. Millis, Science **288**, 468 (2000).
  - [7] J. Zaanen and O. Gunnarson, Phys. Rev. B **40**, 7391 (1989).
  - [8] V.J. Emery, S. A. Kivelson, and H. Q. Lin, Phys. Rev. Lett. **64**, 475 (1990).
  - [9] P. A. Lee, T. M. Rice, and P. W. Anderson, Phys. Rev. Lett. **31**, 462 (1973).
  - [10] R. H. McKenzie, Phys. Rev. B **52**, 16428 (1995).
  - [11] V. Blum, L. Hammer, K. Heinz, C. Franchini, J. Redinger, K. Swamy, C. Deisl, and E. Bertel, Phys. Rev. B **65**, 165408 (2002).
  - [12] A. Menzel, Zh. Zhang, M. Minca, Th. Loerting, C. Deisl, and E. Bertel, New J. Phys. **7**, 102 (2005).
  - [13] K. Swamy, P. Hanesch, P. Sandl, and E. Bertel, Surf. Sci. **466**, 11 (2000).
  - [14] C. Deisl, K. Swamy, N. Memmel, E. Bertel, C. Franchini, G. Schneider, J. Redinger, S. Walter, L. Hammer, and K. Heinz, Phys. Rev. B **69**, 195405 (2004).
  - [15] H. Pfnür, C. Voges, K. Budde, and L. Schwenger, Prog. Surf. Sci. **53**, 205 (1996).
  - [16] S. Hatta, H. Okuyama, T. Aruga, and O. Sakata, Phys. Rev. B **72**, 081406 (R) (2005).
  - [17] K. Swamy, A. Menzel, R. Beer, and E. Bertel, Phys. Rev. Lett. **86**, 1299 (2001).
  - [18] M. Imada, A. Fujimori, and Y. Tokura, Rev. Mod. Phys. **70**, 1039 (1998).